

Reza N. Jazar
Liming Dai *Editors*

Nonlinear Approaches in Engineering Application

Automotive Engineering Problems

 Springer

Nonlinear Approaches in Engineering Application


Reza N. Jazar • Liming Dai
Editors

Nonlinear Approaches in Engineering Application

Automotive Engineering Problems

 Springer

Editors

Reza N. Jazar 
School of Engineering
RMIT University
Melbourne, VIC, Australia

Liming Dai
Industrial Systems Engineering
University of Regina
Regina, SK, Canada

ISBN 978-3-031-53581-9 ISBN 978-3-031-53582-6 (eBook)
<https://doi.org/10.1007/978-3-031-53582-6>

© The Editor(s) (if applicable) and The Author(s), under exclusive license to Springer Nature Switzerland AG 2024

This work is subject to copyright. All rights are solely and exclusively licensed by the Publisher, whether the whole or part of the material is concerned, specifically the rights of translation, reprinting, reuse of illustrations, recitation, broadcasting, reproduction on microfilms or in any other physical way, and transmission or information storage and retrieval, electronic adaptation, computer software, or by similar or dissimilar methodology now known or hereafter developed.

The use of general descriptive names, registered names, trademarks, service marks, etc. in this publication does not imply, even in the absence of a specific statement, that such names are exempt from the relevant protective laws and regulations and therefore free for general use.

The publisher, the authors, and the editors are safe to assume that the advice and information in this book are believed to be true and accurate at the date of publication. Neither the publisher nor the authors or the editors give a warranty, expressed or implied, with respect to the material contained herein or for any errors or omissions that may have been made. The publisher remains neutral with regard to jurisdictional claims in published maps and institutional affiliations.

This Springer imprint is published by the registered company Springer Nature Switzerland AG
The registered company address is: Gewerbestrasse 11, 6330 Cham, Switzerland

Paper in this product is recyclable.

The beauty of nonlinear approaches to engineering problems is that you must be talented to get even a wrong result.

Dedicated to Xinming and Mojgan

Preface

This book is the eighth volume in the series of Nonlinear Approaches in Engineering Applications, organized by the editors. This series is collecting individual application on engineering problems in which the nonlinearity is quite important. Those system have been introduced, and modeled mathematically, in such a way that their nonlinearities have been used to make the system to work better regarding the objectives of the problems.

The nonlinear analysis, techniques, and applications have been developed in the past two to three centuries when the linear mathematical modeling of natural dynamical phenomena appeared not to be exact enough for some practical applications. The positive aspects of linear approximation of dynamic phenomena are simplicity and solvability. Linear approximation of a system provides us with the simplest model acting as the base and standard for which other nonlinear models should approach when the nonlinearities become negligible. Solvability is another positive characteristic of all linear systems. These two characteristics provide us great ability and desire to model dynamic systems linearly. However, the linear model of many systems cannot provide solutions to be good enough approximation of the real system behavior. For such systems, considering nonlinearities of the phenomena is unavoidable. Although the nonlinear approximation of a system provides us with a better and more accurate model, it also provides us with several complications. One of them is that it makes us to search for indirect methods to gain some information of the possible solutions. Due to the nonlinearity and complexity of nonlinear systems, usually, it is very difficult or impossible to derive any analytical and closed-loop solutions for the systems. In solving or simulating the nonlinear systems, we have to rely on approximate or numerical methods, which may only provide approximate results while errors are unavoidable during the processes of generating the approximate results.

Level of the Book

This book aims at engineers, scientists, researchers, engineering, and physics students of graduate levels, together with the interested individuals in engineering, physics, and mathematics. This book focuses on application of the nonlinear approaches representing a wide spectrum of disciplines of engineering and science. Throughout the book, great emphases are placed on engineering applications, physical meaning of nonlinear systems, and methodologies of the approaches in analyzing and solving for the systems. Topics that have been selected are of high interest in engineering and physics. An attempt has been made to expose the engineers and researchers to a broad range of practical topics and approaches. The topics contained in the present book are of specific interest to engineers who are seeking expertise in modern applications of nonlinearities.

The primary audience of this book are researchers, graduate students, and engineers in mechanical engineering, engineering mechanics, electrical engineering, civil engineering, aerospace engineering, mathematics, and science disciplines. In particular, the book can be used for training graduate students as well as senior undergraduate students to enhance their knowledge by taking a graduate or advanced undergraduate course in the areas of nonlinear science, dynamics and vibration of discrete and continuous systems, structure dynamics, and engineering applications of nonlinear science. It can also be utilized as a guide to the readers' fulfillment in practices. The covered topics are also of interest to engineers who are seeking to expand their expertise in these areas.

Organization of the Book

This book is a collection of 10 important problems set in 2 parts: Modeling Dynamic Systems and Applied Dynamic Systems. Both parts are focused on applications of practical engineering problems. There are five chapters in Part 1. Chapter 1 is on three-dimensional nonlinear vibration model and response characteristics of deep-water riser-test pipe system, showing how mechanical vibrations can be used in extracting underground liquids such as water and oil. Chapter 2 deals with model-prototype experiment in vehicle dynamics. Chapter 3 is on flexible mechanisms. Chapter 4 is on modeling and analysis of tire-road separation problem in vehicle vibrations. Chapter 5 is on employing neural network to solve nonlinear differential equations. There are five chapters in Part 2. Chapter 6 is on interesting engineering question from energy point of view, if writing from left to right is better or writing from right to left. This question has been answered by a robotic simulation. Chapter 7 discusses the problems in measurement of the sea level rise. Chapter 8 is on further discussion on problems of sea level rise. Chapter 9 illustrates how game theory can be used in solving engineering problems. Chapter 10 studies the nonlinear pull-in instability problem in micro- and nano-mechanisms.

Each of the chapters covers an independent topic along the line of nonlinear approach and engineering applications of nonlinear science. The main concepts in nonlinear science and engineering applications are explained fully with necessary derivatives in details. The book and each of the chapters are intended to be organized as essentially self-contained. All necessary concepts, proofs, mathematical background, solutions, methodologies, and references are supplied except for some fundamental knowledge well known in the general fields of engineering and physics. The readers may therefore gain the main concepts of each chapter with as less as possible the need to refer to the concepts of the other chapters and references. Readers may hence start to read one or more chapters of the book for their own interests.

Method of Presentation

The scope of each chapter is clearly outlined and the governing equations are derived with an adequate explanation of the procedures. The covered topics are logically and completely presented without unnecessary overemphasis. The topics are presented in a book form rather than in the style of a handbook. Tables, charts, equations, and references are used in abundance. Proofs and derivations are emphasized in such a way that they can be straightforwardly followed by the readers with fundamental knowledge of engineering science and college physics. The physical model and final results provided in the chapters are accompanied with necessary illustrations and interpretations. Specific information that is required in carrying out the detailed theoretical concepts and modelling processes has been stressed.

Prerequisites

The present book is primarily intended for researchers, engineers, and graduate students, so the assumption is that the readers are familiar with the fundamentals of dynamics, calculus, and differential equations associated with dynamics in engineering and physics, as well as a basic knowledge of linear algebra and numerical methods. The presented topics are given in a way to establish as conceptual framework that enables the readers to pursue further advances in the field. Although the governing equations and modelling methodologies will be derived with adequate explanations of the procedures, it is assumed that the readers have a working knowledge of dynamics, university mathematics, and physics together with theory of linear elasticity.

Acknowledgments

This book is made available under the close and effective collaborations of all the enthusiastic chapter contributors who have the expertise and experience in various disciplines of nonlinear science and engineering applications. They deserve sincere gratitude for the motivation of creating such book, encouragement in completing the book, scientific and professional attitude in constructing each of the chapters of the book, and the continuous efforts toward improving the quality of the book. Without the collaboration and consistent efforts of the chapter contributors, the completion of this book would have been impossible. What we have at the end is a book that we have every reason to be proud of.

It has been gratifying to work with the staff of Springer through the development of this book. The assistance provided by the staff members have been valuable and efficient. We thank Springer for their production of an elegant book.

Regina, SK, Canada
Melbourne, VIC, Australia

Liming Dai
Reza N. Jazar

Contents

Part I Modeling Dynamic Systems

Three-Dimensional Nonlinear Vibration Model and Response Characteristics of Deep-Water Riser-Test Pipe System.....	3
Xiaoqiang Guo, Liming Dai, Jun Liu, Qingyou Liu, and Yufa He	
Dealing with Non-linearities in a 1:7 Autonomous Land Vehicle.....	51
Muhammad Rehan Siddiqi, Hormoz Marzbani, and Reza. N. Jazar	
Nonlinear Analysis of Flexible Parallel Mechanisms Through Bézier-Based Integration.....	105
R. Nopour, M. M. Aghdam, and A. Taghvaeipour	
Vibration Analysis of Tire –Road Separation in a Bicycle-Car Model.....	133
Quy Dang Nguyen, Tra Van Nguyen, Dai Quoc Vo, Tuan Ngoc Vu, Sina Milani, Hormoz Marzbani, and Reza N. Jazar	
Physics-Informed Neural Network for Solution of Nonlinear Differential Equations.....	163
Ali Fallah and Mohammad Mohammadi Aghdam	

Part II Applied Dynamic Systems

Energy Analysis of Handwriting with Robotic Analog.....	181
Mingjia Wang, Tegwyn G. Murden, Hettiadura E. T. Fernando, Reza N. Jazar, and M. Mahinfalah	
Computations of Absolute Sea Levels at Tide Gauge Locations Accounting for Variable Subsidence.....	251
Alberto Boretti	
Accounting for Accelerating Subsidence in the Analysis of Tide Gauge Records.....	265
Albert Boretti	

Evolutionary Game Theory and Innovative Building Strategies..... 283
Javad Khazaii, Ali Khazaei, Hamid Khayyam, and Reza N. Jazar

**A Hybrid Numerical Study of the Nonlinear Instability
of Nano-switches**..... 295
M. Bameri, V. Mirzaei, P. Moradweysi, and M. M. Aghdam

Index..... 319

List of Figures

Fig. 1	Failure forms of the riser-test pipe system (RTS). (a) Buckling deformation (b) Fatigue fracture (c) Friction perforation...	7
Fig. 2	Structure diagram of the RTS.....	9
Fig. 3	External fluid forces acting on the riser.....	15
Fig. 4	Contact deformation between the riser and test pipe.....	18
Fig. 5	Schematic of the impact load by high-speed gas.....	20
Fig. 6	Schematic diagram of Newton-Raphson method iteration principle.....	25
Fig. 7	Flow chart of solving nonlinear vibration model of the RTS.....	26
Fig. 8	Experimental system design.....	31
Fig. 9	Experimental system structures. (a) Diagram of experimental pool. (b) Structure diagram of test bench. (c) Schematic diagram of upper and lower boundary joints. (d) Sensor layout diagram.....	32
Fig. 10	Physical diagram of test system. (a) Physical drawing of test bench. (b) Adjusting spring. (c) Tension adjustment device. (d) Bottom universal joint. (e) Gas transportation system. (f) Experimental pool.....	34
Fig. 11	The RMS distribution of riser displacement. (a) The RMS of riser in IL direction (b) The RMS of riser in CF direction.....	35
Fig. 12	The amplitude frequency response curve of riser at measuring point 3. (a) The amplitude frequency response curve of riser in IL direction (b) The amplitude frequency response curve of riser in CF direction.....	36
Fig. 13	The RMS distribution of test pipe displacement. (a) The RMS of riser in IL direction (b) The RMS of riser in CF direction...	37
Fig. 14	The amplitude frequency response curve of test pipe at measuring point 3. (a) The amplitude frequency response curve of test pipe in IL direction (b) The amplitude frequency response curve of test pipe in CF direction.....	38
Fig. 15	Phase trajectories of marine fluid. (a) IL direction (b) CF direction...	40

Fig. 16 Time history response of random wave motion. **(a)** Response of random wave surface **(b)** Wave spectrum..... 42

Fig. 17 Heave displacement of offshore platform..... 43

Fig. 18 Vibration response of the RTS. **(a)** IL direction **(b)** CF direction **(c)** Longitudinal direction..... 44

Fig. 19 Distribution of contact impact and friction forces for the RTS. **(a)** Impact force **(b)** Frictional force..... 45

Fig. 20 Distribution of maximum tensile and compressive stress and strength safety factor of test pipe. **(a)** Maximum tensile stress **(b)** Maximum compressive stress **(c)** Strength safety factor.... 46

Fig. 1 Traxxas XO-1, the 1:7 scaled autonomous land vehicle..... 52

Fig. 2 Stripped Traxxas XO-1 to showcase each and every component of the RC-Car (Traxxas)..... 52

Fig. 3 Shows the battery used to power myRIO..... 54

Fig. 4 MyRIO front view..... 54

Fig. 5 Connection between myRIO port C connector and the SM..... 56

Fig. 6 LabVIEW block diagram code for generating PWM signals for the SM..... 56

Fig. 7 The relationship between the duty cycle and the middle axle steering input for the ALV based on the Ackermann’s condition..... 57

Fig. 8 Screenshot of the Traxxas app on mobile showing the connected vehicle and transmitter with the garage icon highlighted in green from the main menu of the app..... 59

Fig. 9 Screenshot of the Traxxas app on mobile showing the garage menu and the lock/unlock option..... 59

Fig. 10 Castle link V3 connected to ESC..... 59

Fig. 11 Shows the main demo page of the Castle v3link programmer program on computer..... 60

Fig. 12 Shows the advanced options tab and the “Link Live” option..... 60

Fig. 13 Shows the connection between the Arduino Uno and the ESC..... 61

Fig. 14 Shows the idealistic duty cycle values for setting up the 3 points in the ESC for speed control..... 62

Fig. 15 Shows the LabVIEW program for sending a duty cycle signal of 0.080 (neutral PWM signal) for the first 10 seconds whenever the ESC and LabVIEW programs are switched on for driving the ALV..... 63

Fig. 16 Hardware connection between myRIO and the Traxxas rpm sensor..... 64

Fig. 17 LabVIEW code for reading the analog input from the rpm sensor.... 64

Fig. 18 LabVIEW code for recording the rpm of ALV for different intervals of duty cycle only in the forward direction..... 65

Fig. 19 LabVIEW code for calculating the equivalent speed in km/h..... 66

Fig. 20 Shows how to find the X-component of the COM for the naked ALV (not to scale)..... 67

Fig. 21 Illustration of how to shift the X-component of the COM for the ALV (not to scale)..... 68

Fig. 22 Shows how to find the Y-component of the COM for the naked ALV (not to scale)..... 69

Fig. 23 Illustration of how to shift the Y-component of the COM for the ALV (not to scale)..... 69

Fig. 24 Illustration of how the ALV is balanced as a passenger Car and how myRIO COM was aligned with the ALV’s COM..... 70

Fig. 25 Graph showing the result of the oscillations captured during the yaw moment of inertia experiment from time 7–55 seconds on the naked ALV..... 71

Fig. 26 Shows the naked ALV, suspended in mid-air by a group of strings attached to it..... 72

Fig. 27 Shows the connection between the PmodGYRO and myRIO..... 73

Fig. 28 Picture shows that the sensitivity factor of 0.00875 is being multiplied into the raw data of the output..... 74

Fig. 29 Shows the yaw rates measured during the cornering tire stiffness test for the six different steering inputs used..... 74

Fig. 30 LabVIEW code for measuring longitudinal and lateral accelerations using the built-in IMU inside the myRIO..... 75

Fig. 31 Shows the result of one such curve fitting using the magic tire formula (Pacejka, 2005) for the lateral force against the slip angle..... 76

Fig. 32 Opening dashboard page when the myRIO is connected to the computer..... 81

Fig. 33 Shows the myRIO I/O monitor page with only one option available (connected with USB)..... 82

Fig. 34 Shows the myRIO I/O monitor page with both options available (connected with USB and connected over WiFi)..... 83

Fig. 35 Shows the myRIO I/O monitor dashboard test work bench..... 84

Fig. 36 Shows the myRIO hard disk/memory with the “C” folder highlighted by using a red box..... 84

Fig. 37 Shows the myRIO folder “C” and its contents, which contain all the steering profile files saved on the myRIO offline..... 85

Fig. 38 Shows the program page of the LabVIEW version being used..... 85

Fig. 39 Shows where to find the file reading command in LabVIEW..... 86

Fig. 40 The block diagram command used for loading steering profile into the LabVIEW program..... 86

Fig. 41 The block diagram code for sending the steering angles to the SM..... 87

Fig. 42 The block diagram code for sending the PWM signals to the ESC... 87

Fig. 43 The block diagram code for using the wait (ms) command for controlling the sampling rate of the ALV..... 87

Fig. 44 The block diagram code for stopping the loop/ALV at the right time..... 88

Fig. 45	The complete front panel view of the ALV program.....	88
Fig. 46	How to extract data from the ALV LabVIEW program once it has completed a single run.....	90
Fig. 47	How to clear data from the ALV LabVIEW program once it has completed a single run.....	91
Fig. 48	Shows the impact of using the commands “lowpass” and “smooth” on the raw acceleration data.....	92
Fig. 49	Shows the overview of the complete ALV system for the experiment to be conducted in this chapter.....	93
Fig. 50	Shows the SLC accuracy test done at 21.333 km/h for the ALV (simulation 80 km/h).....	94
Fig. 51	Shows the TL accuracy test done at 16 km/h for the ALV (simulation 60 km/h).....	95
Fig. 52	Shows the TL reliability test done at 11.5 km/h for the ALV when the road was dry and the most wet.....	96
Fig. 53	Shows the TL reliability test done at 12 km/h for the ALV when the road was dry and a little wet.....	97
Fig. 54	Shows the area allotted for experimental testing at the RMIT East Bundoora Campus.....	99
Fig. 1	Schematic diagram of the mechanism.....	108
Fig. 2	Graphic of the mechanism.....	109
Fig. 3	Graphic of the mechanism for $0 \leq \theta_2 \leq 360$	110
Fig. 4	Closed path described by center of mass of the connecting rod.....	111
Fig. 5	Closed path described by center of mass of the connecting rod (ADAMS).....	112
Fig. 6	Planar slider crank mechanism.....	116
Fig. 7	Co-ordinate of the slider block for various solution procedures.....	127
Fig. 8	Comparing co-ordinate of the slider block for RK4 and Bézier method.....	128
Fig. 9	Variation of crank and connecting rod angle during 1.6 s maneuver...	128
Fig. 10	Variation of crank and connecting rod angular velocity during 1.6 s maneuver.....	129
Fig. 11	Connecting rod end-point slopes during 1.6 s maneuver (a) first endpoint, q_3 . (b) second endpoint, q_5	129
Fig. 1	Bicycle-car model for a vehicle vibration.....	135
Fig. 2	The frequency response of a front wheel hop.....	138
Fig. 3	The rear wheel hop frequency response.....	139
Fig. 4	The bounce frequency response.....	139
Fig. 5	The pitch frequency response.....	140
Fig. 6	Time response with no separation at both wheels.....	143
Fig. 7	Time response with separation at rear wheel.....	143
Fig. 8	Time response with separation at the wheels.....	144
Fig. 9	Dynamic responses under a no-contact assumption.....	145
Fig. 10	Dimensional phase portraits in a no-contact zone. (a) Front wheel, (b) rear wheel, (c) front wheel, (b) rear wheel.....	145

Fig. 11 Two wheels contacting the road surface..... 150

Fig. 12 Rear wheel separated from the road surface..... 150

Fig. 13 Two wheels separate from the road surface..... 151

Fig. 14 Series of time response..... 151

Fig. 15 Nondimensional phase portraits in a no-contact zone: **(a)** body, **(b)** pitch, **(c)** body, and **(d)** pitch..... 152

Fig. 16 Comparison of phase portraits of the front wheel: **(a)** no separation and **(b)** separation..... 152

Fig. 17 Comparison of phase portraits of the rear wheel: **(a)** no separation and **(b)** separation..... 153

Fig. 18 Vertical velocities in a separation zone..... 153

Fig. 19 Vertical accelerations in a separation zone..... 154

Fig. 20 Phase portraits of acceleration and velocity: **(a)** front wheel, **(b)** rear wheel, **(c)** body, and **(d)** pitch motion..... 154

Fig. 21 Frequency response under a no-separation assumption..... 155

Fig. 22 Frequency response of the body and two wheels..... 156

Fig. 23 The relative frequency response with one separation point..... 156

Fig. 24 Frequency response with pitch motion..... 157

Fig. 25 Separation with two periods..... 157

Fig. 26 Separation duration of the front wheel and that of the rear wheel..... 158

Fig. 27 Separation duration of both wheels together..... 159

Fig. 28 Separation duration following the position of the mass center..... 159

Fig. 29 Separation duration for the damping ratios..... 160

Fig. 30 Separation durations for stiffness ratios..... 160

Fig. 31 Separation durations for mass ratios..... 161

Fig. 1 The geometry of the Euler-Bernoulli beam..... 168

Fig. 2 **(a)** Deflection of simply supported beam under uniform load ($\bar{q} = 10$), **(b)** loss function value during the training procedure..... 170

Fig. 3 **(a)** Convergence of natural frequency of beam during the training procedure for different values of initial guess of natural frequency, **(b)** the mode shape of vibration for the different values of initial guess..... 170

Fig. 4 **(a)** Convergence beams natural frequency for different function employed to create required extra information, **(b)** Vibration shape modes of beam for different functions employed to create required extra information..... 171

Fig. 5 **(a)** Convergence beams buckling load for different function employed to create required extra information, **(b)** Buckling shape modes of beam for different functions employed to create required extra information..... 172

Fig. 6 **(a)** Comparison between the PINN and MATLAB BVP4C for nonlinear bending of SS beam, **(b)** Deflection of beam with various boundary condition using PINN and BVP4C ($\bar{q} = 10$). ($N_H = 3, N_D = 20, A_{\text{Func}} = \tanh, N_I = 40,000$)..... 173

Fig. 7	(a) Comparison between the PINN and MATLAB ODE45 for slightly damped Van der Pol equation ($N_H = 3$, $N_D = 500$, $N_B = 100$, $A_{\text{Func}} = \tanh$, $N_I = 30,000$), (b) Comparison between the PINN and MATLAB ODE45 for highly damped Van der Pol equation ($N_H = 4$, $N_D = 1500$, $N_B = 200$, $A_{\text{Func}} = \tanh$, training iteration = 40,000).....	174
Fig. 8	(a) Comparison between the PINN and exact solution for heat transfer problem, (b) Temperature distribution domain in x and t domain ($N_H = 3$, $N_D = 2500$, $N_B = 240$, $A_{\text{Func}} = \tanh$, training iteration = 40,000).....	175
Fig. 1	Dimensions of a person. (First in Architecture 2023).....	189
Fig. 2	Anatomical arm in the Y-Z plane (side profile).....	190
Fig. 3	Anatomical right-handed robot in the X-Y plane (top down).....	190
Fig. 4	Anatomical left-handed robot in the X-Y plane (top down).....	190
Fig. 5	General sinusoidal path along the X, Y, and Z planes.....	197
Fig. 6	General sinusoidal path along the X-Y plane.....	197
Fig. 7	Left-to-right sinusoidal waveform, drawn with the right hand.....	200
Fig. 8	Left-to-right sinusoidal waveform with higher frequency, drawn with the right hand.....	201
Fig. 9	Lowercase o stroke order and orientation on the X-Y plane.....	202
Fig. 10	Lowercase b stroke order and orientation on the X-Y plane.....	202
Fig. 11	Lowercase t stroke order and orientation with isometric view on the left and top down X-Y plane view on the right.....	204
Fig. 12	Stroke order and final orientation for <i>Robot</i> Note: The order of strokes is as follows for each new letter: pink -> lavender -> light green -> orange -> yellow -> light blue. Furthermore, dotted black lines denote the transfer lines between each letter.....	205
Fig. 13	Schematic of 3R articulated robot used to represent the human arm with a locked wrist.....	207
Fig. 14	Flowchart of model design.....	215
Fig. 15	Joint variables determined through path data.....	221
Fig. 16	Joint velocities determined by joint variables.....	221
Fig. 17	Joint acceleration determined by joint velocities.....	221
Fig. 18	Joint torques.....	222
Fig. 19	Theta1 recalculated through ODE45.....	222
Fig. 20	Theta2 recalculated through ODE45.....	222
Fig. 21	Theta3 recalculated through ODE45.....	223
Fig. 22	Theta1 recalculated through ODE89.....	223
Fig. 23	Theta2 recalculated through ODE89.....	224
Fig. 24	Theta3 recalculated through ODE89.....	224
Fig. 25	Theta 1 recalculated through Euler's method.....	225
Fig. 26	Theta 2 recalculated through Euler's method.....	225
Fig. 27	Theta 3 recalculated through Euler's method.....	225
Fig. 28	Theta 1 recalculated through ODE45.....	228

Fig. 29 Theta 2 recalculated through ODE45..... 228

Fig. 30 Theta 3 recalculated through ODE45..... 228

Fig. 31 Theta1 recalculated through ODE89..... 229

Fig. 32 Theta2 recalculated through ODE89..... 229

Fig. 33 Theta3 recalculated through ODE89..... 230

Fig. 34 Theta1 recalculated through Euler’s method..... 230

Fig. 35 Theta2 recalculated through Euler’s method..... 230

Fig. 36 Theta3 recalculated through Euler’s method..... 231

Fig. 37 Theta1 recalculated through ODE45..... 233

Fig. 38 Theta2 recalculated through ODE45..... 233

Fig. 39 Theta3 recalculated through ODE45..... 233

Fig. 40 Theta1 recalculated through ODE89..... 234

Fig. 41 Theta2 recalculated through ODE89..... 234

Fig. 42 Theta3 recalculated through ODE89..... 234

Fig. 43 Theta1 recalculated through Euler’s method..... 235

Fig. 44 Theta2 recalculated through Euler’s method..... 235

Fig. 45 Theta3 recalculated through Euler’s method..... 236

Fig. 1 Sydney Fort Denison subsidence. GPS values for $z(t)$ and estimation of v_z from (geodesy.unr.edu/NGLStationPages/stations/FTDN.sta). The GPS dome is co-located with the tide gauge..... 255

Fig. 2 Fremantle subsidence. GPS values for $z(t)$ and estimation of v_z from (geodesy.unr.edu/NGLStationPages/stations/UWA0.sta; geodesy.unr.edu/NGLStationPages/stations/WLT1.sta; geodesy.unr.edu/NGLStationPages/stations/HEN2.sta). These GPS domes are relatively far from the tide gauge..... 256

Fig. 3 Sydney Fort Denison sea level. Values for $y(t)$ and estimation of v_y from (sealevel.info/MSL_graph.php?id=Sydney).... 257

Fig. 4 Fremantle sea level. Values for $y(t)$ and estimation of v_y from (sealevel.info/MSL_graph.php?id=fremantle)..... 257

Fig. 5 Analysis of the Fremantle relative sea level. (Data from psmsl.org/data/obtaining/rlr.monthly.data/111.rlrdata)..... 258

Fig. 6 Analysis of the Sydney relative sea level. (Data from psmsl.org/data/obtaining/rlr.monthly.data/196.rlrdata; psmsl.org/data/obtaining/rlr.monthly.data/65.rlrdata)..... 258

Fig. 7 Modelled subsidence in Sydney..... 261

Fig. 8 Modelled subsidence rate in Fremantle..... 261

Fig. 9 Absolute mean sea levels in Sydney Fort Denison..... 262

Fig. 10 Absolute mean sea levels in Fremantle..... 262

Fig. 1 Subsidence rates at about 2300 tide gauge locations **(a)**, and in all the GPS locations **(b)** as described in (Hammond et al. 2021). **(c)** is a map of world subsidence from the results of **(b)**. Image **(a)** is from [42]. Image **(b)** is from (geodesy.unr.edu/vlm/FigureVelocities.png). Image **(c)** is from (geodesy.unr.edu/vlm/FigureVLM_resamp.png). Credit Nevada Geodetic Laboratory..... 268

Fig. 2 GIA subsidence rates as computed in (Paulson et al. 2007). Image from (en.wikipedia.org/wiki/Post-glacial_rebound#/media/File:PGR_Paulson2007_Rate_of_Lithospheric_Uplift_due_to_post-glacial_rebound.png). Public domain..... 269

Fig. 3 Velocity and acceleration of absolute (top) and relative sea levels (b). Supporting data is in the appendix..... 277

Fig. 1 Schematic of a cantilever and doubly clamped NEM switch..... 303

Fig. 2 Displacement per dimensionless voltage using TL method with different step numbers..... 313

Fig. 3 Displacement per dimensionless voltage using the RK method with different step numbers..... 313

Fig. 4 Displacement per dimensionless voltage using AB method with different step numbers..... 314

Fig. 5 Displacement in terms of dimensionless voltage using the BZ method with different step numbers..... 314

Fig. 6 Effect of TS and nonlocal parameters on the instability voltage..... 316

List of Tables

Table 1	Simulated experiment parameters.....	29
Table 2	Calculation parameters of BY5-2-1 well.....	39
Table 1	Physical characteristics of myRIO and its battery	55
Table 2	Relationship between duty cycle and steering of the ALV.....	58
Table 3	Relationship between the duty cycle and the speed of the ALV	65
Table 4	All required parameters of the ALV	66
Table 5	Moment of inertias (I_z) for ALV and its components.....	71
Table 6	Information of each component system to calculate I_z	72
Table 7	Cornering tire stiffness of the front and rear wheels of the ALV...	77
Table 8	All required parameters for dimensional analysis of the ALV	77
Table 9	All parameters of the simulated passenger car	78
Table 10	Calculated Π groups for the simulation car	80
Table 11	SLC accuracy test done at 21.333 km/h for the ALV (simulation 80 km/h).....	94
Table 12	TL accuracy test done at 16 km/h for the ALV (simulation 60 km/h).....	95
Table 13	TL reliability test done at 11.5 km/h for the ARC-car when the road was dry and the most wet.....	97
Table 14	TL reliability test done at 12 km/h for the ALV when the road was dry and a little wet.....	97
Table 1	Dimensional parameters of a bicycle-car model.....	138
Table 1	Pseudocode for cubic.m.....	194
Table 2	Pseudocode for qtcpath.m.....	195
Table 3	Pseudocode for Sine_graph_path_generation.m.....	198
Table 4	Pseudocode for lowercaseb_ltr.m.....	203
Table 5	Pseudocode for lowercaset_ltr.m.....	204
Table 6	Pseudocode for robot_full_pathing.m.....	205
Table 7	Pseudocode for reloparc.m.....	206
Table 8	Denavit–Hartenberg parameter table for 3R articulated robot.....	208

Table 9	Pseudocode for main_3R.m in the MATLAB file.....	216
Table 10	Pseudocode for Eulers_Method_3R_robot.m in the MAPLE file.....	217
Table 11	Pseudocode for ODE45_3R_Robot.m from the MATLAB file.....	219
Table 12	Pseudocode for myode3.m in the MATLAB file.....	219
Table 13	Comparison and verification of energy calculated for the solvers.....	226
Table 14	Energy consumed for writing direction and writing orientation....	227
Table 15	Comparison and verification of energy calculated for the methods.....	231
Table 16	Comparison and verification of energy calculated for the methods.....	232
Table 17	Energy consumed for writing direction and writing orientation....	237
Table A.1	Pseudocode for generating text file by using sinusoidal path as an example.....	243
Table A.2	Image of text file showing the first 10 rows of the text file.....	243
Table C1	Energy values calculated by using joint variables.....	245
Table C2	Energy values calculated by using joint velocities.....	246
Table 1	Relative and absolute sea levels and land velocities and accelerations.....	271
Table 1	Evolutionary game, dove-dominated environment.....	287
Table 2	Evolutionary game – Hawk Dominated Environment.....	288
Table 3	Evolutionary game – Traditional vs innovative construction models.....	289
Table 1	Bézier method formula for different orders (Aghdam et al. 2015).....	310
Table 2	Abbreviations guideline.....	312
Table 3	The values of pull-in instability with and without fringe field effect.....	312
Table 4	The number of cycles and the values of initial conditions errors for each method.....	315
Table 5	Instability voltage for each method per different MoA cycles.....	316

Part I
Modeling Dynamic Systems

Three-Dimensional Nonlinear Vibration Model and Response Characteristics of Deep-Water Riser-Test Pipe System



Xiaoqiang Guo, Liming Dai, Jun Liu, Qingyou Liu, and Yufa He

Abbreviations

3D	three-dimensional
BOP	blowout preventer
CF	crossflow
CFD	computational fluid dynamics
IL	inline
RMS	root mean square
RTS	riser-test pipe system
VIV	vortex-induced vibration

X. Guo (✉) · J. Liu

School of Mechatronic Engineering, Southwest Petroleum University, Chengdu, China

School of Mechanical Engineering, Chengdu University, Chengdu, China

e-mail: 202099010174@swpu.edu.cn

L. Dai

Industrial Systems Engineering, University of Regina, Regina, SK, Canada

Q. Liu

State Key Laboratory of Oil and Gas Reservoir Geology and Development Engineering, Chengdu, China

Y. He

CNOOC Research Institute Co., Ltd., Beijing, China

© The Author(s), under exclusive license to Springer Nature Switzerland AG 2024

R. N. Jazar, L. Dai (eds.), *Nonlinear Approaches in Engineering Application*,

https://doi.org/10.1007/978-3-031-53582-6_1

Nomenclature

m^*	mass ratio of riser
E	elastic modulus of the RTS, Pa
$v'_i, i = x, y, z$	first-order derivative of riser displacements versus z
$\dot{v}_i, i = x, y, z$	first-order derivative of riser displacements versus time
ρ_v	density of the riser, kg/m^3
$F_x(z, t)$	contact/impact force of riser-test pipe in x -directions, N
$F_z(z, t)$	friction force of riser-test pipe in z -directions, N
$F_L(z, t)$	lateral lift in the CF direction, N
ω_v	natural angular frequency of riser
L_v	length of riser, m
D_o	riser outer diameter, m
m_i	the mass of the gas per unit length (kg)
$S_i, i = x, y, z$	displacement components of the test pipe, m
$S''_i, i = x, y, z$	second derivative of test pipe displacements versus z
$f_x(z, t)$	high-speed fluid impact load in test pipe in x -direction, N
$f_z(z, t)$	high-speed fluid impact load in test pipe in z -direction, N
ω_s	natural angular frequency of test pipe
$w_s(=m_s g)$	weight of test pipe per unit length, N
V_r	relative velocity between the fluid and the riser, m/s
U_c	outflow velocity of the riser, m/s
F_D', C_D	component forces of the fluctuating drag force and corresponding coefficient
$q_i, i = x, y$	dimensionless wake oscillator variables in IL and CF directions
S_t	Strouhal number
$R_i, i = 1, 2$	radius of riser and test pipe, m
$\omega_i, i = 1, 2$	axial displacements of the riser and test pipe, m
$E_i, i = 1, 2$	elastic modulus of the riser and test pipe material, Pa
$q(x)$	uniform load distribution for riser and test pipe, N
ρ_i	density of gas in the test pipe, kg/m^3
$\alpha(t)$	deflection angles of test pipe in x -direction, rad
$\alpha(s)$	inclination angle, rad
K_U	rotational stiffness of the upper flexible joint
$u_{\text{boat}}(t)$	heave displacement of the platform, m
m_p	mass of platform, kg
$\eta(t)$	surface displacement of random wave, m
$\hat{\omega}_i$	circular frequency of the i th harmonic, Hz
a_i	amplitude of the i th harmonic component, m
$S(\omega)$	random wave spectrum
ω	circular frequency, Hz
$T_{1/3}$	significant period of the wave, s
T_p	peak period of the wave, s
σ	peak shape coefficient

$F_p(t)$	exciting force of the random wave on the heave plate
$J_1(\cdot)$	first order Bessel function of first kind
z_{plate}	depth of heave plate, m
\mathbf{d}	displacement vector of riser unit
$\varphi_i, i = x, y, z$	vibration shape function of riser and test pipe unit
$\mathbf{F}(t)$	load column vector
$\mathbf{M}(t)$	matrices of the overall mass
ρ_p	density of the actual RTS
ρ_m	density of the RTS in the simulation experiment
λ	radial similarity ratio
$u_i, i = x, y, z$	displacement components of riser, m
A_v	cross-sectional area of the riser, m ²
$u_i'', i = x, y, z$	second derivative of riser displacements versus z
I_v	polar moment of inertia of the riser, m ⁴
m_v	mass of the per unit length riser, kg
$F_y(z, t)$	contact/impact force of riser-test pipe in y -directions, N
$c_v(=2m_v\omega_v\zeta)$	structural damping coefficient of riser
$F_D(z, t)$	drag force in the IL direction, N
w_g	buoyant weight of riser per unit length, N
ρ_w	density of the sea-water, kg/m ³
A_s	cross-sectional area of the test pipe, m ²
m_s	mass of the per unit length test pipe, kg
$S'_i, i = x, y, z$	first-order derivative of test pipe displacements versus z
$\dot{S}_i, i = x, y, z$	first-order derivative of test pipe displacements versus time
$f_y(z, t)$	high-speed fluid impact load in test pipe in y -direction, N
$c_s(=2m_s\omega_s\zeta)$	structural damping coefficient of test pipe
$v_i, i = x, y, z$	absolute velocities of the internal high-speed fluid (m/s)
V	fluid flow velocity in the test pipe, m/s
\overline{C}_d	coefficient of steady-state drag force
\overline{C}_l	coefficient of steady lift force
F_L', C_L	fluctuating lift force and corresponding coefficient
$z_i, i = 1, 2$	radial distance from the contact point of pipe to the inner wall of riser, m
ω'_s	vortex shedding frequency
r	horizontal distance from the contact point to the test pipe axis, m
F	contact load of riser-test pipe, N
$\mu_i, i = 1, 2$	Poisson's ratio of riser and test pipe material
ξ	friction coefficient between the riser and test pipe
A_i	cross-sectional area of the wellbore, m ²
$\varphi(t)$	deflection angles of test pipe in y -direction, rad
$\varphi(s)$	azimuth, rad
K_L	rotation stiffness of the BOP

$B_i, i = 1, 2$	heave radiation and heave viscous damping
A_w	area of the platform at sea level, m^2
\overline{F}_z	random heave wave exciting force on platform, N
ε_i	initial phase of the i th harmonic component, rad
$\Delta\omega$	frequency step
f	Frequency, Hz
$H_{1/3}$	significant wave height, m
f_p	peak frequency of the wave, Hz
γ	peak parameter
R	platform radius, m
$F_s(t)$	exciting force of the random wave on the platform body
d	draft of platform, m
B_{plate}	width of heave plate, m
$\bar{\mathbf{d}}$	displacement vector of test pipe unit
\mathbf{D}	matrix of overall displacement
$\mathbf{K}(t)$	matrices of the overall stiffness
$\mathbf{C}(t)$	matrices of the overall damping
E_p	elastic modulus of the actual RTS
E_m	elastic modulus of the RTS in the simulation experiment

1 Introduction

With the increasing demand for oil and gas resources in the world, the exploitation trend of offshore oil and gas resources gradually develops from shallow water (water depth is less than 500 m) to deep water (water depth is between 500 m and 1500 m). The riser-test pipe system (RTS) is the core equipment for deep-water oil and gas exploitation but the weakest equipment. Compared with conventional water depth testing conditions, the RTS is subjected to greater risks in deep-water test conditions; these risks are mainly caused by severe non-periodic vibrations of the riser and test pipe (RTS) induced by the vortex induced effect on riser, flow-induced effect on test pipe, nonlinear contact/collision of the tube in tube, and longitudinal/transverse coupling effect, thereby making the RTS more susceptible to buckling deformation (Fig. 1a), fatigue fracture (Fig. 1b), and friction perforation (Fig. 1c) (Zhou et al. 2013). Once the system structure is damaged, it will lead to serious offshore oil and gas accidents, resulting in significant economic losses and environmental pollution. Therefore, the three-dimensional (3D) nonlinear vibration model and response characteristics for deep-water RTS should be investigated.

In early vortex-induced vibration (VIV) studies, most of the work focused on rigid cylinders (Sarpkaya 1979; Govardan and Williamson 2000; Bearman 2003), in which the general VIV mechanism and law, such as the frequency-locked phenomenon (Dahl et al. 2010) and lagging behavior (Facchinetti et al. 2004). In recent years, driven by offshore oil and gas exploitation, more and more attention

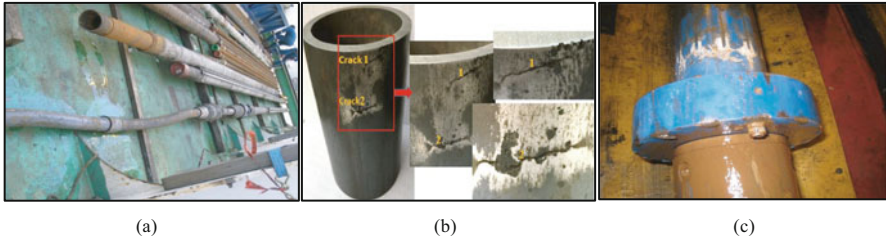


Fig. 1 Failure forms of the riser-test pipe system (RTS). (a) Buckling deformation (b) Fatigue fracture (c) Friction perforation

has been paid to the VIV problem of flexible cylinders in which the aspect ratio is a very important parameter. Physical experiments (Chaplin et al. 2005; Trim et al. 2005; Vandiver et al. 2009; Huera-Huarte et al. 2014; Gao et al. 2015) and computational fluid dynamics (CFD) numerical simulations (Newman and Karniadakis 1997; Bourguet et al. 2011, 2013; Mao et al. 2019, 2020) are the two most common methods in these studies, and remarkable progress was made. However, when the aspect ratio of a cylinder is large or a solid model is used, physical experiments usually become very expensive and impractical, and CFD numerical simulation is too time-consuming and difficult. Therefore, in the VIV study of risers, there are relatively few works that consider a large aspect ratio or the actual size. In addition to a large aspect ratio, the impact of the ocean environment load on the VIV behavior of a riser is significant. The VIV response mechanism of a flexible riser under shear flow was examined by Mathelin and Langre (2005) using a wake oscillator model presented by (Facchinetti et al. 2004). Since the VIV amplitude in the crossflow (CF) direction is larger than that in the inline (IL) direction, most work has focused on the VIV in the CF direction (Khalak and Williamson 1999). The effects of the flow velocity, top tension, and pipe diameter on VIV behavior in the crossflow direction of a riser were studied by Xu et al. (2017) and He et al. (2017) using a VIV model. In the above studies, the VIV behavior in the IL direction and its influence were not taken into account. However, it was found in the work of Jauvtis and Williamson (2003) that as the mass ratio $m^* (=4m_s/\rho\pi D^2)$, the ratio of the structural quality to the mass of discharged fluid was less than 6.0, and the IL vibration of a cylinder could not be neglected. The VIV characteristics study of a rigid cylinder presented by Gu et al. (2016), Martins and Avila (2019) and Gao et al. (2019) also showed that the effect of the IL vibration was significant. In our recent work (Liu et al. 2018a, b, 2019), the response characteristics of VIV of marine risers with consideration of the coupling effects of the CF and IL vibration were investigated. It was found that the frequency locking effect in the uniform flow and the multi frequency effect in the shear flow for the IL vibration.

Vibration of tubular structure caused by inside flow has attracted some researchers' attentions. In the early research, preliminary research was conducted on string vibration under the action of internal flow (Aitken 1878), and initially confirmed the phenomenon of pipe vibration induced by fluid in pipe without

elaborating the interaction mechanism between fluid and pipe (Shilling and Lou 1980). Subsequently, many scholars carried out detailed research on the string vibration model, and established the calculation method of fluid force (Deng 2006), the string vertical vibration (Paidoussis et al. 2008; Ju and Tong 2014), the lateral vibration (Zhang and Miska 2003; Bagdatli 2015), and the fluid-structure coupled vibration model (Dai et al. 2014; Yu 2017). In recent years, some scholars (Xing and Liang 2015; Li 2016; Liu et al. 2018a, b) have found that the longitudinal/lateral coupling effects of slender tubular columns cannot be ignored. Aimed at the static contact problems of slender structures, a few researchers (Hong et al. 1982; Ding et al. 1989; Shen and Ding 1990; Zhang and Song 2015) have tried to give the calculation methods of contact force between a beam and support structure, and the correctness of the methods was verified by experimental data. Moreover, the bracing effect of the outer pipe was taken into account by some researchers (Tan 2005; Wang et al. 2015; Li 2017) to analyze the static buckling deformation of a tubing string. About the dynamic contact/collision problem of slender structures, the commercial software such as ANSYS and ABAQUS were used by researchers (Zhu et al. 2007; Liu et al. 2016; Yang et al. 2016) to investigate the impact force and friction force in the flow-induced vibration of slender structures in vertical well. Also, in our recent work (Liu et al. 2020; Guo et al. 2021a, b), the flow-induced nonlinear vibration model of tubing string in conventional oil and gas wells was established using micro-finite element and energy methods along with the Hamilton variational principle, which considers the longitudinal/lateral coupling effect of tubing string and the nonlinear contact collision effect of tubing-casing. In summary, the interaction between riser and test pipe is ignored in the above studies, which make the calculation results by the single vibration model not in accordance with the actual. Especially in the deep water test condition, with the increase of length diameter ratio, the interaction between riser and test pipe cannot be ignored.

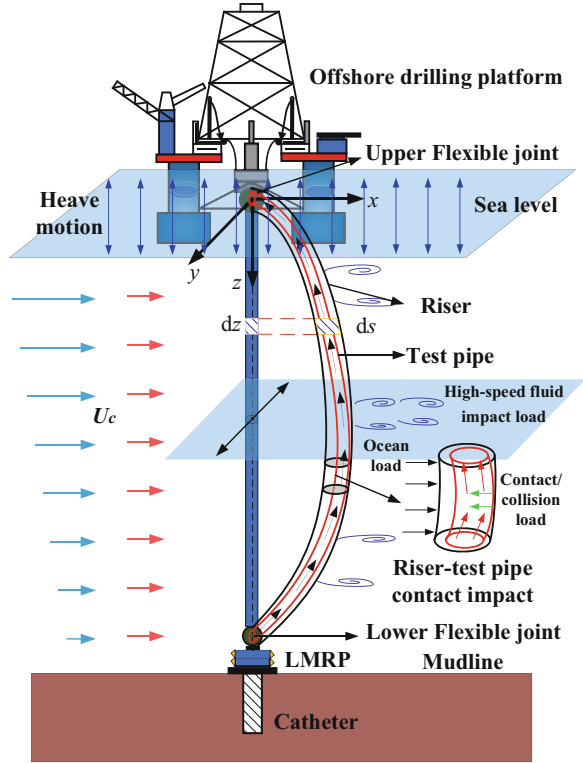
In this study, the 3D nonlinear vibration model of deep-water RTS is established. The Lagrange and cubic Hermite functions are used to discretize the governing equations. Then, the incremental form of Newmark- β and Newton-Raphson are used to solve the 3D nonlinear vibration model. Meanwhile, a vibration test bench for the RTS is designed using similarity principle, and the correctness and effectiveness of the proposed 3D nonlinear vibration model are verified by comparing with experimental data. Finally, the vibration characteristics of the RTS in the South China Sea are analyzed.

2 3D Nonlinear Vibration Model of the RTS

2.1 *Nonlinear Vibration Control Equation of the RTS*

In this section, the 3D vibration control equations of infinitesimal riser-test pipe (RTS) were established through the energy method and Hamilton variational

Fig. 2 Structure diagram of the RTS



principle. The infinitesimal segment of the RTS is too short, such that it can be regarded as a straight segment. Therefore, a coordinate system is established in which the depth direction is set as z -axis, the horizontal direction (the IL direction) is set as x -axis and the y -axis (the CF direction) satisfies the right-hand rule (Fig. 2). The following basic assumptions are made before modeling.

- ① The mechanical property of the material of riser and test pipe is ideal isotropic and elastic.
- ② The gravity and frictional resistance are evenly distributed on the tubing element.
- ③ The test pipe axis is coincided with the riser axis at initial moment, and the gravity of the RTS acts on itself at initial moment.
- ④ The friction coefficient at each location of the system is constant.

(1) Vibration control equation of riser

Based on the small deformation hypothesis and the Kirchhoff hypothesis (Liu et al. 2019), the three displacement field components u_1 , u_2 , and u_3 along the coordinates x , y , and z , respectively, can be written as: